Hindawi
Journal of Sensors
Volume 2019, Article ID 2469647, 12 pages
https://doi.org/10.1155/2019/2469647

Research Article

Investigation of Applicability of an Embedded EM Sensor to Measure the Tension of a PSC Girder

Junkyeong Kim,[1] Ju-Won Kim,[2] and Seunghee Park[1,2]

[1]*Department of Convergence Engineering for Future City, Sungkyunkwan University 2066, Seobu-ro, Jangan-gu, Suwon-si, Gyeonggi-do 16419, Republic of Korea*
[2]*School of Civil & Architectural Engineering, Sungkyunkwan University 2066, Seobu-ro, Jangan-gu, Suwon-si, Gyeonggi-do 16419, Republic of Korea*

Correspondence should be addressed to Seunghee Park; shparkpc@skku.edu

Received 29 October 2018; Revised 31 December 2018; Accepted 10 January 2019; Published 31 March 2019

Academic Editor: Carlos Ruiz

This study investigates the applicability of an embedded EM sensor using a series of experimental studies. To verify the embedded EM sensor, the magnetic hysteresis of various types of PS tendons is measured. After that, the embedded EM sensor is embedded into the concrete and the possibility of obtaining measurements is verified. Finally, the downscaled PSC girder specimen having a sheath with a different curvature is fabricated and the influence of the sheath curvature is investigated. The magnetic hysteresis was changed constantly even though the type of PS tendon was changed, and the embedded EM sensor can measure the magnetic hysteresis, even in the concrete and curved sheath. The area of magnetic hysteresis was decreased according to the increase in the tension force, but the actual values were different according to the number and cross-sectional area of tendons and the initial state of sensors. To compensate for the measured data, the tensile force was converted to the tensile stress and the area ratio was used to compensate for the initial value of the EM sensor. According to the test results, the embedded EM sensor could be applied to the actual PS girder and it can measure the actual tension, which includes the friction loss.

1. Introduction

Structural health monitoring (SHM) has become a very important process with the aging of constructed infrastructure worldwide. Nondestructive evaluation (NDE) is a reliable method that is employed to monitor the state of health of civil structures [1–4]. Since the first posttensioned concrete bridge was built in 1936, many prestressed concrete (PSC) bridges have been widely constructed globally. However, as PSC bridges age, the tensile forces in the prestressing strands weaken owing to a variety of losses, including instantaneous losses such as elastic shortening, friction, and anchorage sets, which occur at the time of transfer of the prestressing force, as well as time-dependent losses owing to steel relaxation, and the concrete creep and shrinkage that occur after transferring the prestressing force and during the lifetime of the member. A PSC bridge can collapse suddenly if the prestressing force becomes lower than the designed tensile force [5, 6]. Thus, to perform SHM of PSC bridges, monitoring of the tensile forces of PSC bridges is very important.

Various NDE methods have been developed to estimate the tensile force of PS tendons or cables for bridges. Field measurements have been performed by attaching sensors such as a tension measuring gauge (Tensmeg), directly to the outside of the PS tendon or indirectly by sensing the strain near the tendon using an electrical strain gauge and vibrating wire strain gauge (VWSG) installed in the concrete or on a rebar near the duct [7]. More recently, various NDE methods for measuring tensile forces have been studied using techniques that are based on guided stress waves [8, 9], the system identification technique based on modal parameters [10], the impedance method applied to an anchorage plate [11], the use of the in-strand encapsulated fiber Bragg grating (FBG) sensor [12, 13], the use of stress-sensitive and magnetic field-tunable microwave composites

with embedded short ferromagnetic microwire inclusions [14], and the noncontact stress monitoring method using Fe-based microwires [15].

The magnetic-based tensile force estimation methods were studied using magnetic sensors. The elastomagnetic (EM) sensor was used to measure steel cables of cable-stayed bridges [16], and experiments were performed to verify the permeability changes according to the stress and temperature [17]. To measure the magnetic responses of PS tendons that do not appear outside the PSC girder, an embedded EM sensor was proposed [18]. The embedded EM sensor consists of bobbin, primary coil, and secondary coil. The primary coil generates the magnetic field to the PS tendon and the secondary coil measures the magnetic flux caused by the magnetized PS tendon. The magnetic hysteresis loop is changed by the inverse effect of magnetostriction; as the stress is introduced to the PS tendon, the domain structure under the effect of applied stresses is changed and these phenomenon leads the change of magnetic hysteresis of the PS tendon [19, 20].

This study investigates the applicability of the developed embedded EM sensor through series of experimental studies to apply it to the actual construction site. The influence of the type of PS tendon, concrete cover, and curvature of sheath was verified through series of experimental studies.

2. Variations in Magnetic Hysteresis according to Tensile Force on Various PS Tendons

The materials and methods should contain sufficient details so that all procedures can be repeated. It may be divided into headed subsections if several methods are described. The PS tendons that induce tensile forces on the PSC girder were produced as types A to D, according to the KS D 7002 standard (Table 1).

Among them, the 7-wired PS tendons are primarily used for PSC girders. The target tensile strength of A-type PS tendons is 1720 N/mm^2, that of B-type tendons is 1860 N/mm^2, that of C-type tendons is 2160 N/mm^2, and that of D-type tendons is 2400 N/mm^2. According to the standard relaxation value, normal relaxation tendons have the suffix "N" and low-relaxation tendons have the suffix "L."

For each tendon type, here are differences in the physical properties, such as the tensile load and yield load, for each tendon type, which cause differences in the magnetic hysteresis variation with the tensile force. Type B tendons are primarily used for PSC bridges, and types C and D are used for high-performance bridges because of their high tensile force tolerance. Therefore, in this study, the variations in magnetic hysteresis according to the tensile force of three types of PS tendons (B, C, and D) were measured using the embedded EM sensor.

2.1. Experimental Setup. The magnetic hysteresis of three types of PS tendons, which was affected by a stepwise tensile force variation introduced by a universal testing machine (UTM), was measured using the embedded EM sensor to verify the variation of the magnetic hysteresis according to the type of PS tendon. The specimens consisted of three B-type PS tendons with lengths of 1.5 m and diameters of 12.7 mm, three C-type PS tendons with lengths of 1.5 m and diameters of 15.2 mm, and three D-type PS tendons with lengths of 1.5 m and diameters of 15.2 mm to confirm the magnetic hysteresis variation according to the type of PS tendon and diameter. The basic properties of each specimen are listed in Table 2.

Table 1: KS D 7002 Standard.

Kind	Label
2 wired	SWPC2N, SWPC2L
3 wired	SWPD3N, SWPD3L
7 wired	
A type	SWPC7AN, SWPC7AL
B type	SWPC7BN, SWPC7BL
C type	SWPC7CL
D type	SWPC7DL
19 wired	SWPC19N, SWPC19L

The experiments were performed by installing each specimen and embedded EM sensor in the UTM, as shown in Figure 1, after which stepwise tensile forces (0, 50, 100, 150, and 180 kN) were introduced to each specimen. The magnetic hysteresis was measured three times at each tensile force step. The input signal was a ±3 V triangular wave with a frequency of 0.02 Hz.

3. Result of Magnetic Hysteresis according to the Type of PS Tendon and Tensile Force

The variations of the magnetic hysteresis with the tensile force are shown in Figure 2. The magnetic hysteresis curves confirm that the area of hysteresis decreases as the tensile force increases, irrespective of the type of PS tendon.

To quantify the variations in the area of hysteresis according to the tensile force change, the area of hysteresis was extracted and is plotted in Figure 3. The area of hysteresis quantitatively decreased, while the tensile force gradually increased. This occurs because the magnetization of the PS tendon decreased as the stress was introduced into the tendon.

Linear regression was used to determine the relationship between the area of hysteresis and the tensile force, and the regression result is shown in Figure 4. The relationship between the area and tensile force is nonlinear because it involves many factors, such as the maximum magnetic flux density or coercive force, unlike the magnetic permeability, which is extracted only from the slope of the hysteresis. In addition, the change in the area of the hysteresis curves according to the change in the tensile force was different for each type of PS tendon. Thus, the area of the hysteresis curve is highly sensitive to changes in the physical properties and cross-sectional area of the tendon.

Table 2: Basic properties of each type of PS tendon.

Type of PS tendon	Diameter (mm)	Nominal cross-sectional area (mm^2)	Unit weight (kg/km)	Tensile load (kN)	Yielding load (kN)	Elongation (%)	Relaxation (%)
B type (SWPC7BL)	12.7	98.71	774	183	156	3.5	2.5
C type (SWPC7CL)	15.2	138.7	1101	300	255	3.5	2.5
D type (SWPC7DL)	15.2	138.7	1101	333	283	3.5	2.5

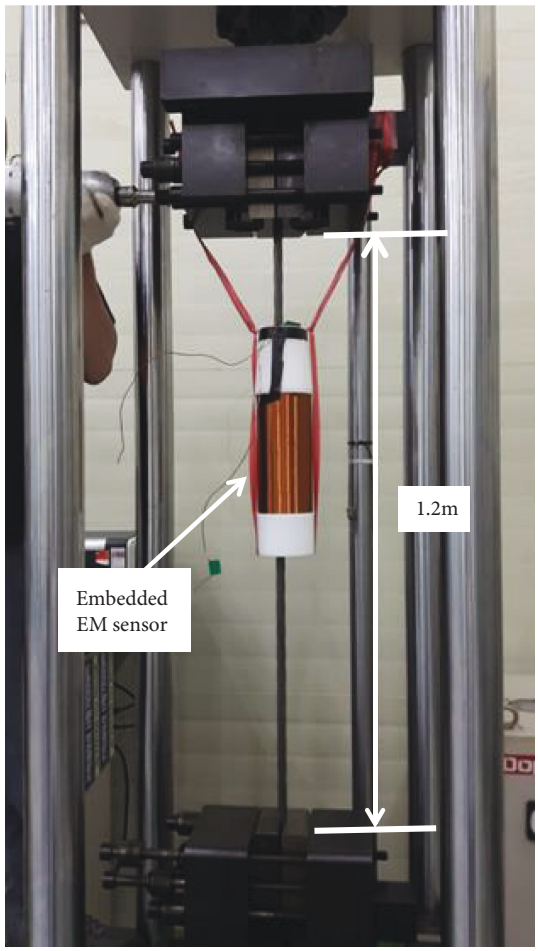

Figure 1: Experimental setup for tensile force measurement test.

4. Verification of Built-In Potential for an Embedded EM Sensor in a PSC Girder

Because embedded EM sensors are installed inside PSC girders, it should be possible for them to work in concrete. Therefore, tests were performed to verify whether the tensile force of PS tendons can be measured even after embedding the EM sensors in concrete.

4.1. Experimental Setup. To verify the potential for embedding EM sensors in concrete, a small PSC specimen was constructed, as shown in Figure 5. A total of two specimens were fabricated, and the thickness of the concrete covering was varied to determine the possibility of realizing a signal change depending on the thickness of the concrete covering the sensor.

To reduce the error with the tensile force measured on the load cell installed on the left side of the specimen, the embedded EM sensor was installed as close as possible to the left anchor block of the test specimen, as shown in Figure 6. The sheath of each specimen was installed linearly to minimize the effect of friction between the sheath and tendon. After the installation of the embedded EM sensor, the concrete was poured, as shown in Figure 7, after assembling the basic reinforcing bars. After curing for 34 days after pouring, seven PS tendons were installed on each specimen and the tensile force was introduced. For each specimen, the tensile force was introduced in four steps, as shown in Table 3. The introduced tension was measured using a load cell installed on the left side of the test body. The input signal for magnetic hysteresis measurement was a 0.02 Hz triangular wave of ±3 V.

4.2. Result of the Embedding Test. Figure 8 shows the magnetic hysteresis curves measured for each specimen. It was confirmed that the change in the hysteresis curves according to the tensile force change can be measured using the embedded EM sensor, even when the sensor is in concrete. In addition, it can also be seen that the area of hysteresis decreased with increasing tensile force.

To quantify the change in the area of magnetic hysteresis with the increase in tensile force, the graph was extracted and is plotted in Figure 9.

The area of the hysteresis curve also showed a tendency to decrease as the tensile force increased. To quantitatively confirm this trend, linear regression analysis was performed on the area and tensile force, as shown in Figure 10.

The regression analysis shows that both specimens had similar patterns of change but the rate of change was different. This is caused by differences in the specifications of each sensor embedded in each specimen based on the fact that the initial permeability and the area of hysteresis values of the two specimens were different at the initial state (0 kN). The embedded EM sensor was a type in which the primary coil and the secondary coil were wound around a bobbin, which was manufactured in the same manner, and it was difficult to completely wind the same number of coils (error of approximately 10 turns). The difference between the initial values of the two sensors was caused by this variation, which should be compensated for in order to measure the tensile force reliably.

Based on this experimental study, it was confirmed that the magnetic hysteresis change caused by the variation of

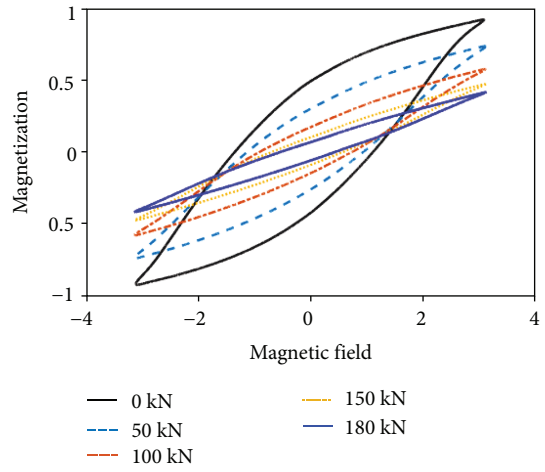

(a) B type—12.7 mm

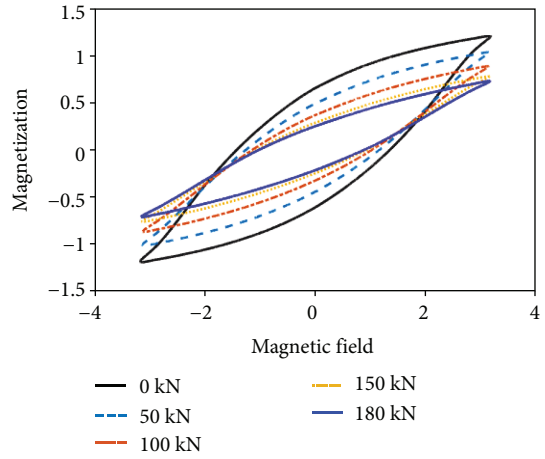

(b) C type—15.2 mm

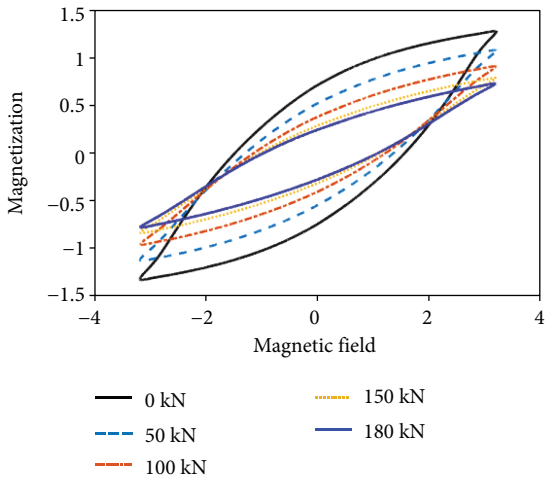

(c) D type—15.2 mm

Figure 2: Magnetic hysteresis change for PS tendons.

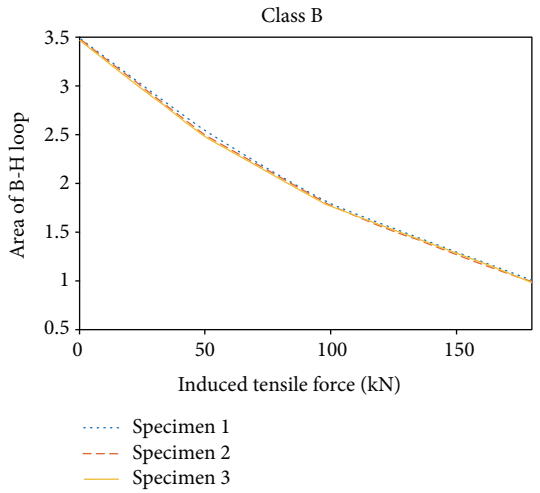

(a) B type (12.7 mm)

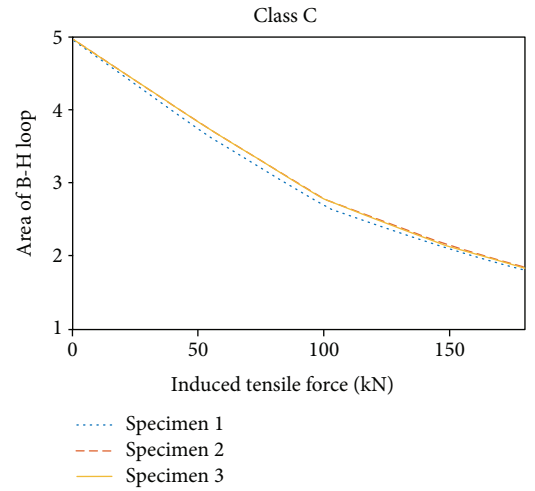

(b) C type (15.2 mm)

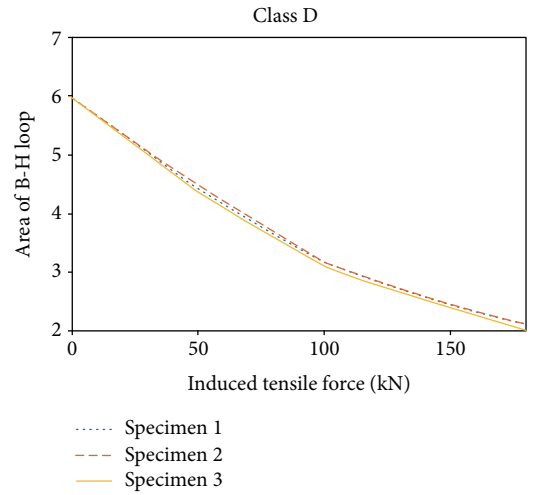

(c) D type (15.2 mm)

Figure 3: Variations in the area of hysteresis with changes in the tensile force for various types of PS tendons.

the tensile force of PS tendons can be measured, even if the embedded EM sensor is buried in concrete. Also, the thickness of concrete did not influence the change of the magnetic hysteresis curve according to the increase of tensile force. It is confirmed that the area of the B-H loop should be

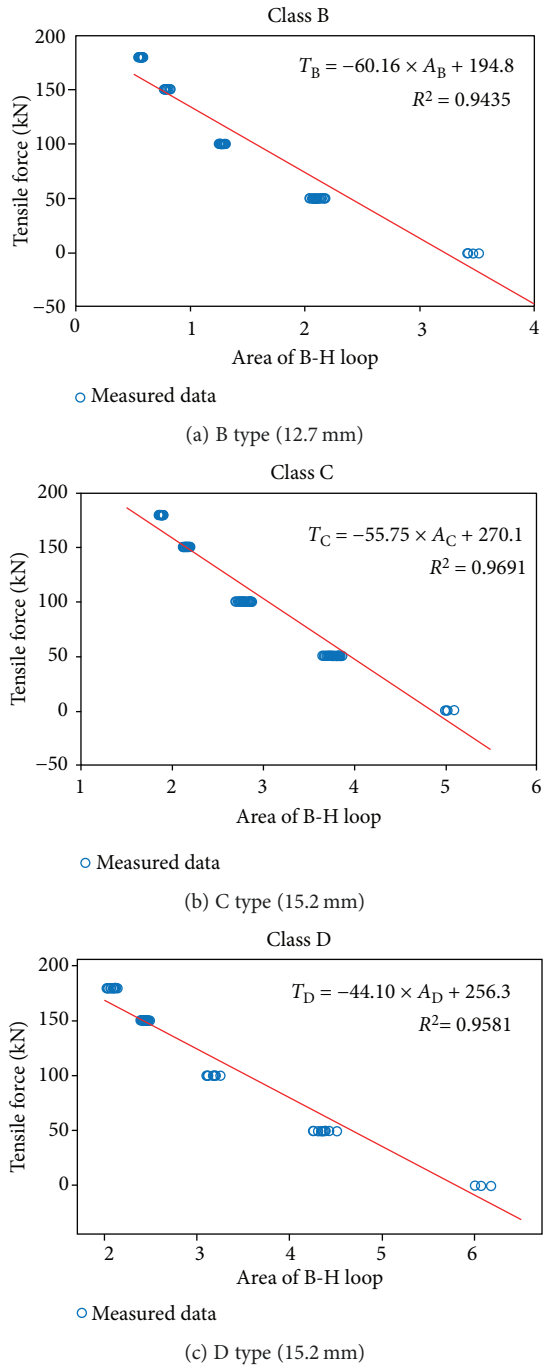

(a) B type (12.7 mm)

(b) C type (15.2 mm)

(c) D type (15.2 mm)

Figure 4: Relationship between area and tensile force according to tendon type.

compensated for according to the differences in embedded EM sensors.

5. Experiment Using a Scaled PSC Girder to Verify the Influence of Sheath Curvature

Experiments were carried out to verify the influence of the curvature of sheath using a scaled PSC girder model with an embedded EM sensor.

5.1. Experimental Settings. Scaled 6 m long PSC girders were fabricated, as shown in Figure 11, and tensile force measurements were performed to verify the applicability of the developed embedded EM sensor. A total of three small girder specimens were fabricated, and the embedded EM sensors were installed on the left anchorage and maximum eccentric parts of each girder, as shown in red in Figure 11. The primary coil (1.2 t PEW enamel copper wire) of each sensor was wound approximately 300 turns, and the secondary coil (0.3 t PEW enamel copper wire) was wound approximately 120 turns. To determine the influence of the eccentricity on the tensile force measurement using the embedded EM sensor, each girder specimen had different sheath curvatures.

After installation of the embedded EM sensor on the sheath, the sensor cables were taken out of the left end and then the concrete was poured into the specimens. After curing of the concrete, four PS tendons (15.2 mm in diameter, B type, 7-wired) were installed in each specimen and load cells were installed on the left anchorage of each specimen. The tensile force was introduced in five steps (100 to 500 bar according to the pressure gauge of the hydraulic jacking machine). The magnetic hysteresis using the embedded EM sensor and reference tensile force using the load cell were measured at each tensile force step. A power integrator, which involves a power amplifier, integrator, and DAQ, was used to measure the magnetic hysteresis of PS tendons using the embedded EM sensor. The power integrator was designed and manufactured for application in the field by reducing the measurement time and equipment size. The conventional DC-based measuring instrument used a 0.02 Hz triangular wave as an input signal, which took about 70 s to measure the hysteresis curve once, whereas the power integrator took about 1 s to perform one measurement using a 1 Hz sine wave. The input signal to measure magnetic hysteresis was a ±3 V, 1 Hz sine wave, and measurements were repeated five times at each tensile force step.

5.2. Result of Experiment on the Scaled PSC Girder Model. Figures 12–14 show the measurement results of the hysteresis curves of the scaled PSC girder specimens. The magnetic hysteresis curves of the PS tendons could be measured using the embedded EM sensor in the PSC girder, and it was confirmed that the area of the hysteresis curves decreased as the tensile force increased. This shows the same pattern as the previous experiment and indicates that the introduction of stress in the longitudinal direction of the PS tendons prevents them from being magnetized. It was also confirmed that the magnetic hysteresis curves of the PS tendons inside the girders can be measured smoothly using the embedded EM sensor, irrespective of the sheath curvature.

The areas of the hysteresis curves were extracted to quantitatively evaluate the change in magnetic properties caused by the change in tension force. Figure 15 shows the change in the area of hysteresis with increasing tensile force. The area of the magnetic hysteresis curve quantitatively decreased with the increasing tensile force. In particular, the area of the B-H loop, which is inversely proportional to the tensile force, of the maximum eccentric part showed a different tendency according to the curvature change of

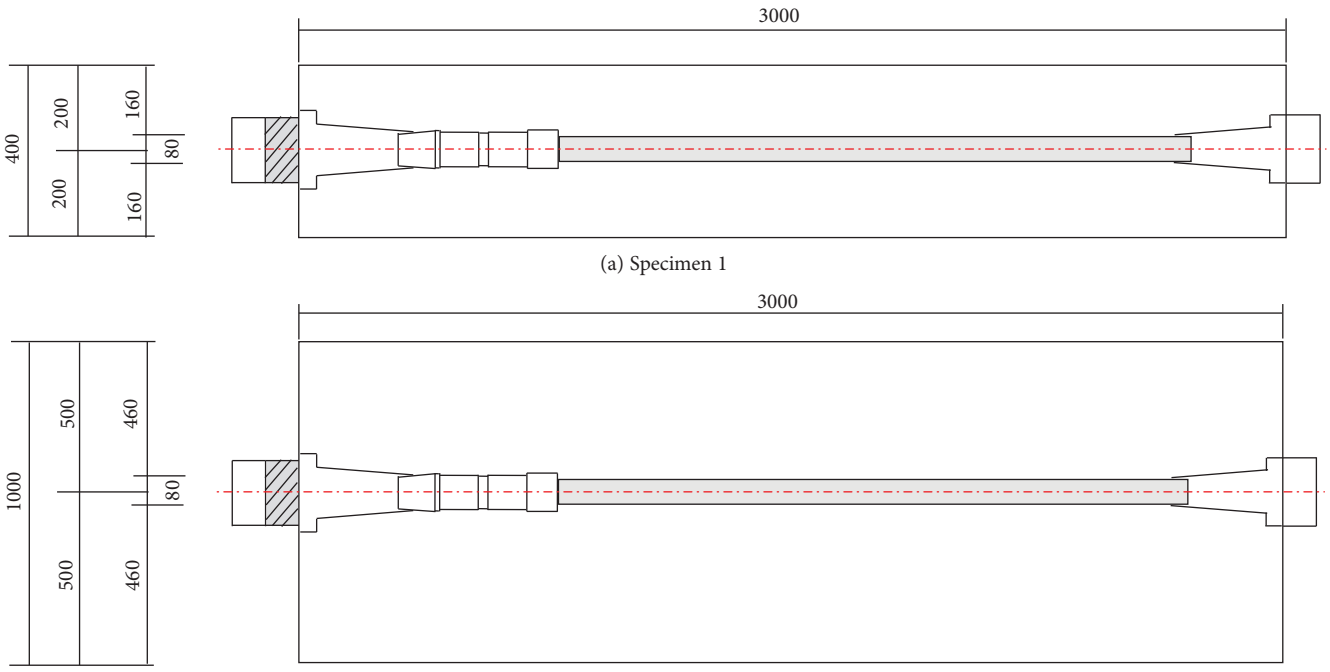

Figure 5: Specimens for sensor embedding test.

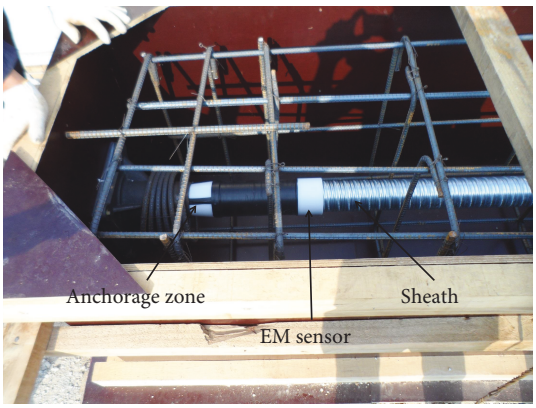

Figure 6: Installation of embedded EM sensor.

Figure 7: Pouring of concrete.

Table 3: Tensile force steps.

Step	Tensile force (kN)	
	Specimen 1	Specimen 2
1	0	0
2	240	250
3	740	730
4	1100	1100

specimens. According to the measurement result, the tensile force of the maximum eccentric point was gradually decreased according to the increase in the curvature. This was caused by the decreased friction between the sheath and PS tendon, and the embedded EM sensor can measure the actual tensile force at the center of the PSC girder.

Figure 16 shows the regression analysis results for the area of hysteresis measured by the sensor of the anchorage part, adjacent to the load cell, and the load cell data to confirm the relationship between the measured tensile force and the area of the hysteresis curve. In the scaled PSC girder test, the area of hysteresis also decreased with the increasing tensile force, which is similar to the previous experimental results.

6. Compensation of Data for General Estimation

6.1. Compensations for the Cross-Sectional Area and Number of PS Tendons. The number and cross-section of PS tendons depend on the PSC girder span length and design load. As in the experimental test results in Section 3, the estimated tensile force (in kN) varies according to the number and

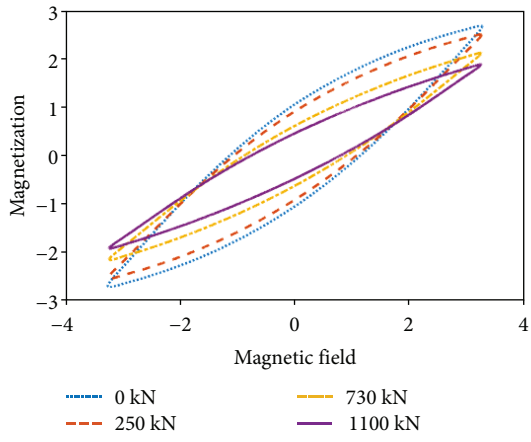

(a) Specimen 1

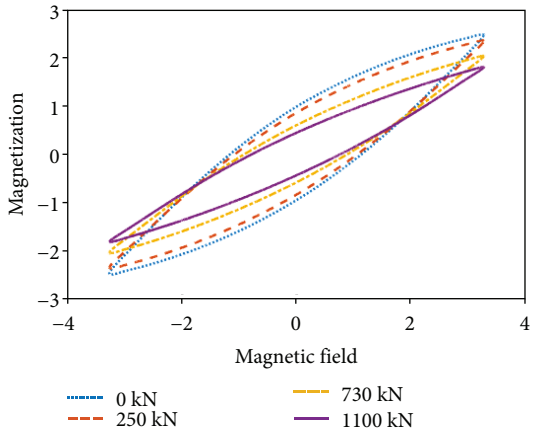

(b) Specimen 2

Figure 8: Variations in magnetic hysteresis curve according to the changes in tensile force in the embedding test.

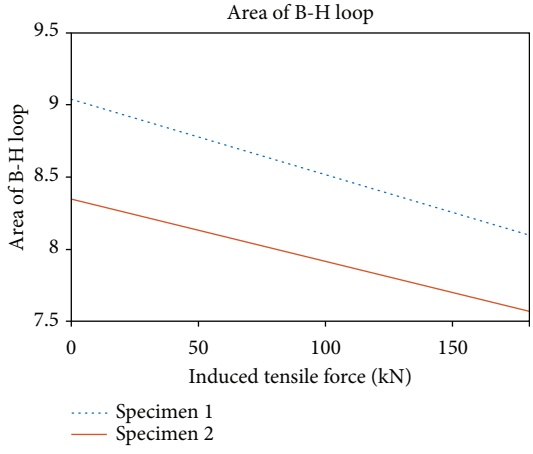

Figure 9: Variations in the area of hysteresis with tensile force in the embedding test.

cross-sectional area of the PS tendon and corrections are necessary to address this problem. To enable corrections for the number and cross-sectional area of PS tendons, the stress

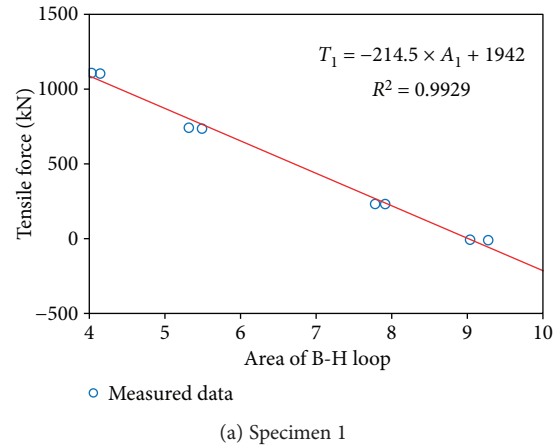

(a) Specimen 1

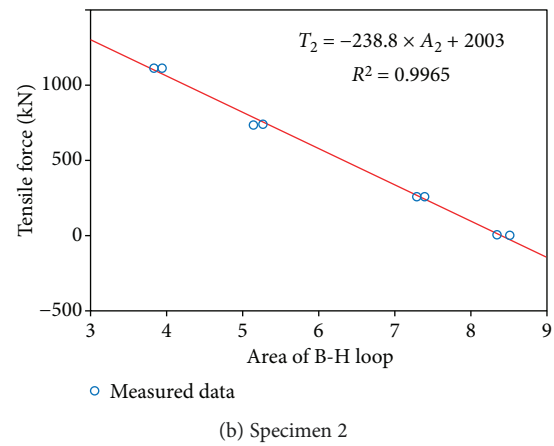

(b) Specimen 2

Figure 10: Relationship between the area of hysteresis and tensile force in the embedding test.

unit, MPa, was used to estimate the tensile force instead of kN.

$$\sigma\,(\text{MPa}) = \frac{1000\,T(\text{kN})}{A_n(\text{mm}^2)\cdot N_T}, \tag{1}$$

where A_n is the nominal cross-sectional area of a PS tendon and N_T is the number of PS tendons per sheath.

Differences associated with the number and nominal cross-sectional area of PS tendons can be corrected for by estimating the stress applied to PS tendons as explained above, which improves the in situ applicability of the proposed estimation method.

6.1.1. Compensation for the Sensor's Initial Value. Because embedded EM sensors were fabricated by winding the primary and secondary coils around a bobbin, differences can occur in the number of turns and state of the coil. For this reason, the initial value (PS = 0) of each sensor has its own eigenvalue and requires relevant correction, as verified in earlier experiments.

This study used the area ratio based on the ratio between the areas at the time of measurement and the baseline to correct for the initial value of the magnetic hysteresis curve

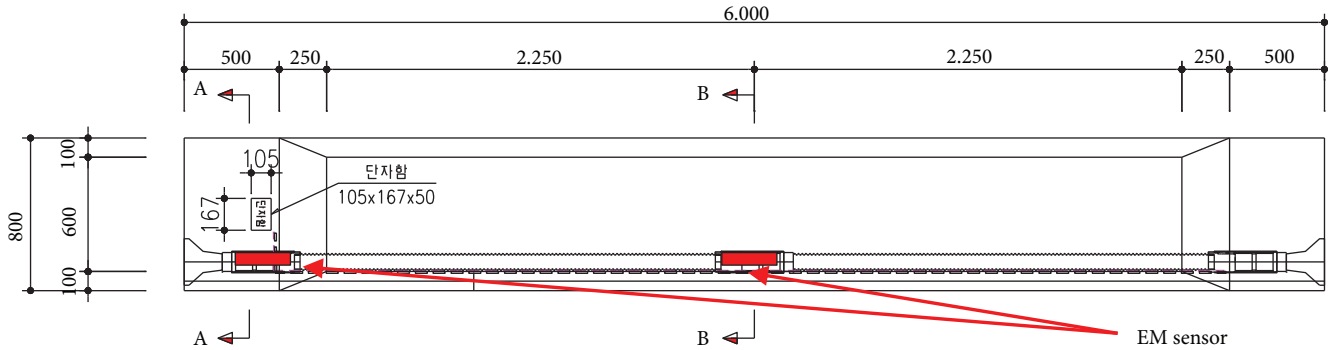

(a) Curvature of sheath: 0

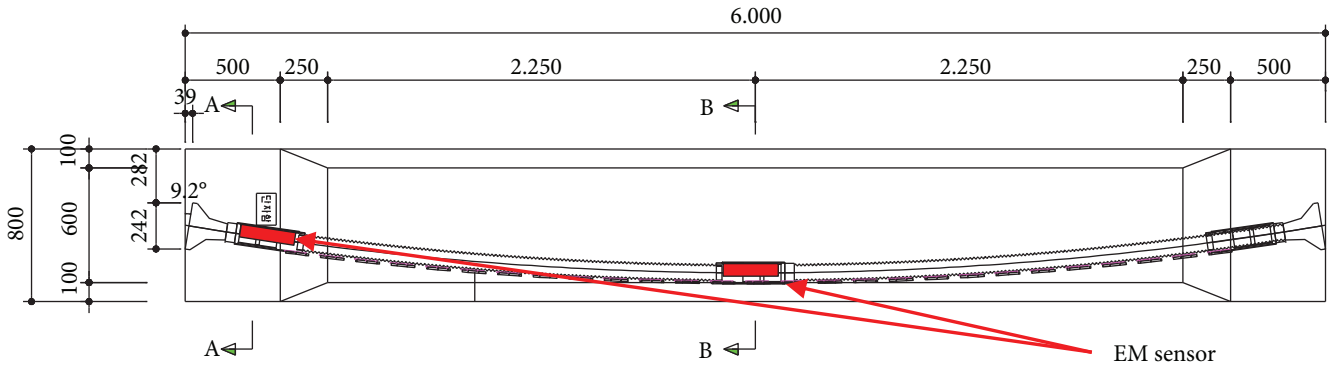

(b) Curvature of sheath: 0.31267

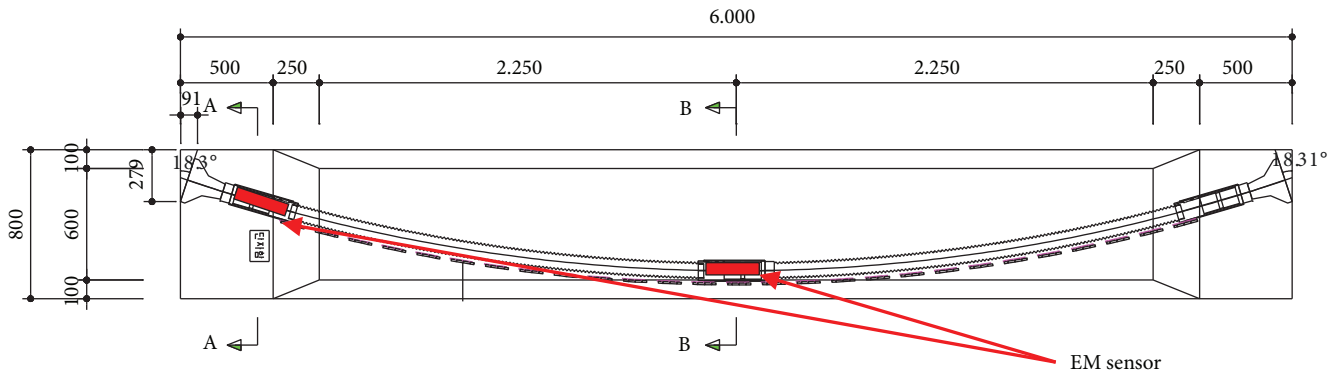

(c) Curvature of sheath: 0.74733

Figure 11: Diagram of scaled PSC girder specimens.

area for each sensor [18]. Equation 2 was used for the area ratio calculation.

$$A_r = \frac{A_0 - A_i}{A_0}, \tag{2}$$

where A_0 is the initial magnetic hysteresis curve ratio and A_i is the magnetic hysteresis curve ratio measured at the ith tensile force measurement. This correction contributes to increasing tensile force estimation accuracy by reducing the error associated with the difference in the number of turns of the coil in different sensors and the error due to the installation environment.

Figure 17 presents the area ratio relative to the stress experimentally tested in Section 3. From these results, it was verified that almost identical results were yielded for different specimens because of the corrections for the sensor's initial value, as well as the number and cross-sectional area of PS tendons. This allows the conclusion that more accurate tensile force estimation is possible without respect to the differences in the sensor and PS tendons by applying the proposed correction methods.

7. Conclusion

This study investigated the applicability of an embedded EM sensor, which can be embedded in a PSC girder, for use with actual PSC girders. To verify the embedded EM sensor, the change in the hysteresis based on the tendon type was investigated and its potential for being embedded in concrete was

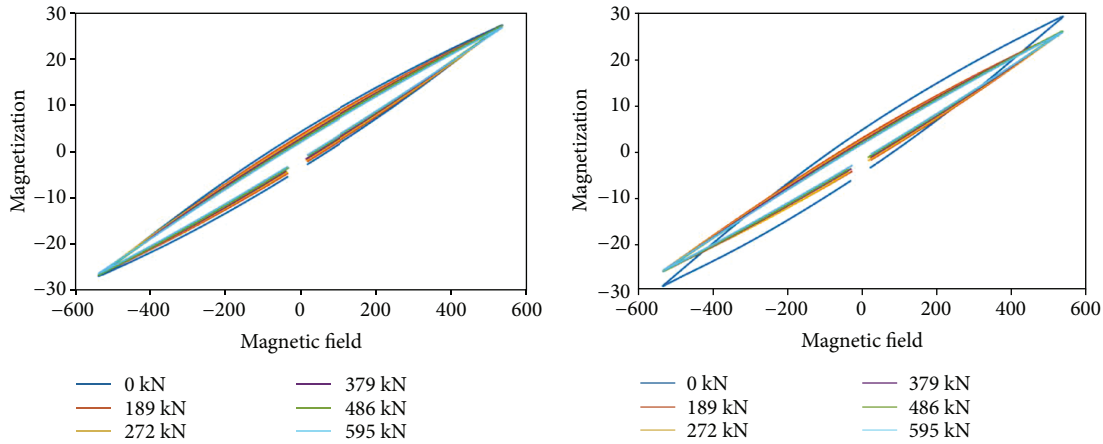

(a) Anchorage part (b) Maximum eccentric part

Figure 12: Variations in magnetic hysteresis depending on tensile force—specimen 1.

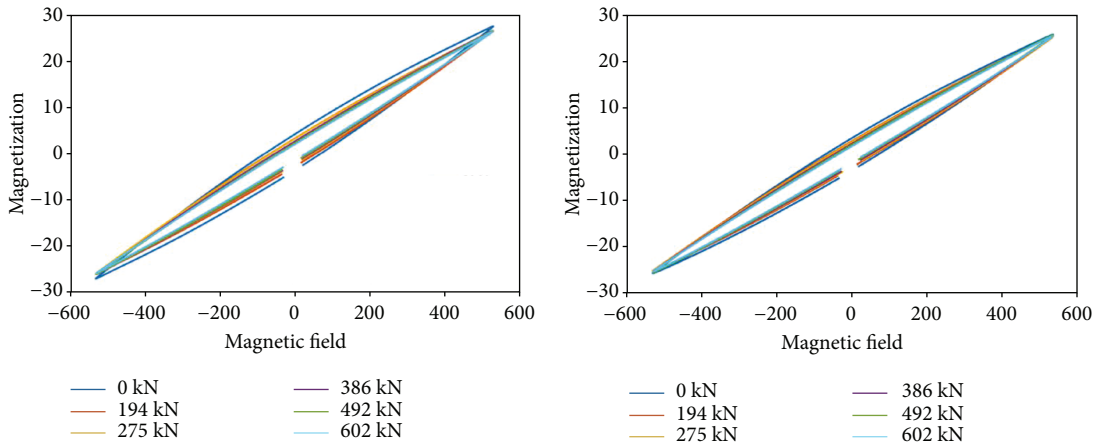

(a) Anchorage part (b) Maximum eccentric part

Figure 13: Variations in magnetic hysteresis depending on tensile force—specimen 2.

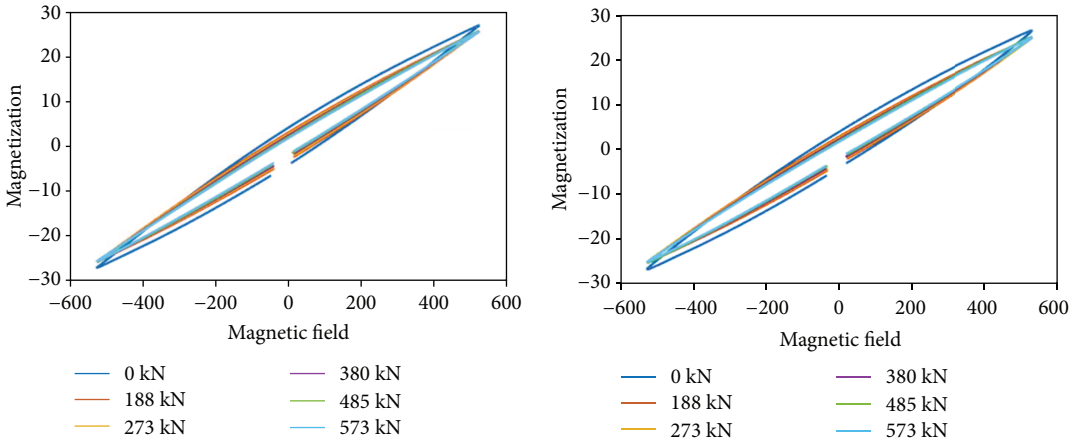

(a) Anchorage part (b) Maximum eccentric part

Figure 14: Variations in magnetic hysteresis depending on tensile force—specimen 3.

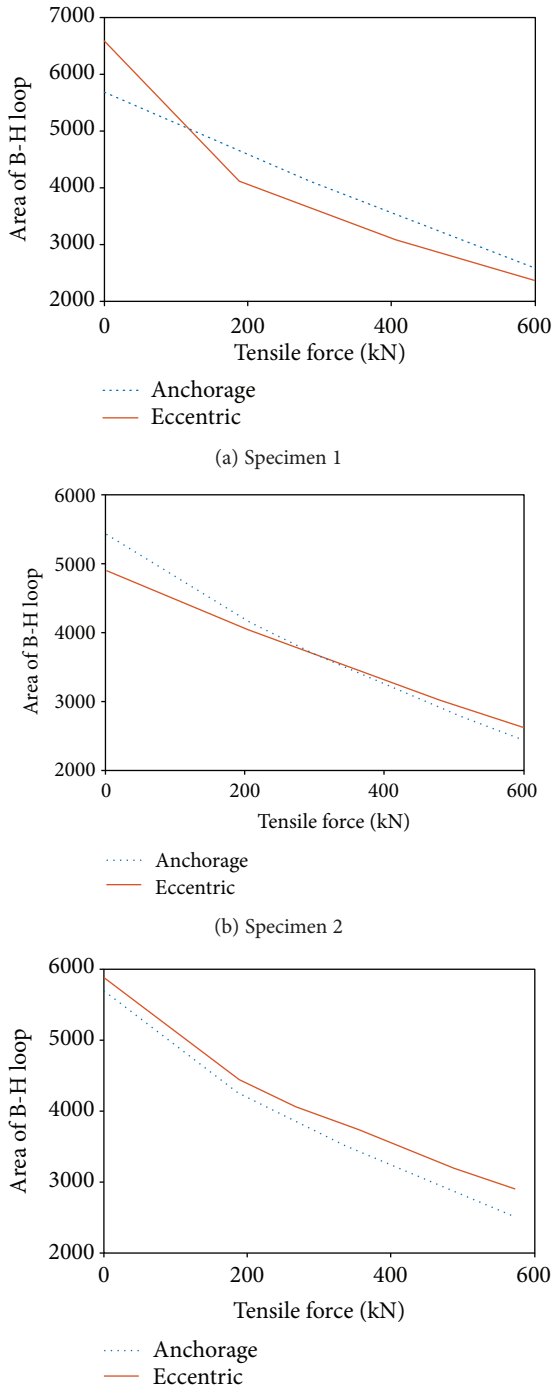

Figure 15: Variation in the area of hysteresis with tensile force in the scaled PSC girder test.

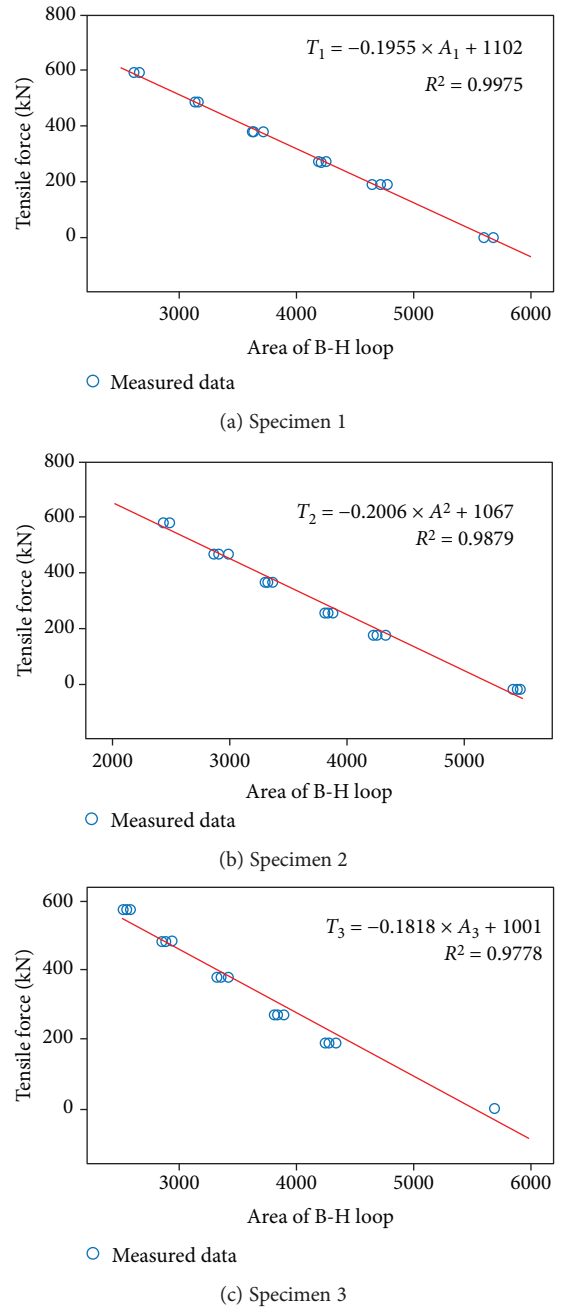

Figure 16: Relationship between the area of hysteresis and tensile force in the scaled PSC girder test.

examined. In addition, the influence of the sheath curvature was examined by performing scaled PSC girder tests. The magnetic hysteresis was decreased according to the increase of tensile forces on the PS tendon irrespective of the type of PS tendon. The area of magnetic hysteresis was proportionally decreased according to the increase in the tension force, but the rate of change was different because of the difference of mechanical properties of PS tendons. And it was confirmed that the embedded EM sensor can measure the magnetic hysteresis even in concrete and even when installed to the curved sheath. In particular, the area of the magnetic hysteresis was decreased nonlinearly in the curved sheath because of the friction loss between the PS tendon and sheath. The friction loss can be measured using an embedded EM sensor which is installed in the maximum eccentric part of the PSC girder.

To compensate for the difference in the measured data, the tensile force was converted to tensile stress. Through the difference caused by the number and cross-sectional area of PS, tendons can be compensated. Also, the area of

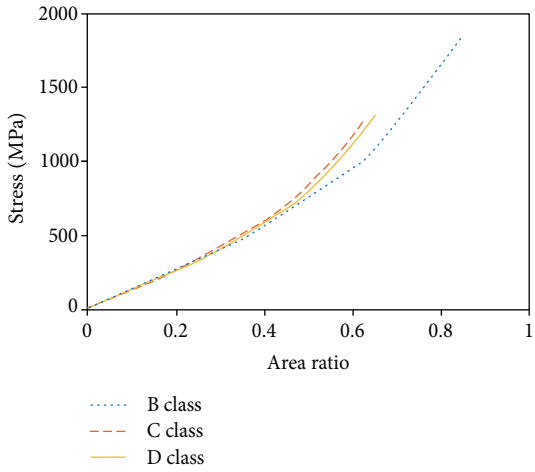

(a) Result of the test on various types of PS tendons

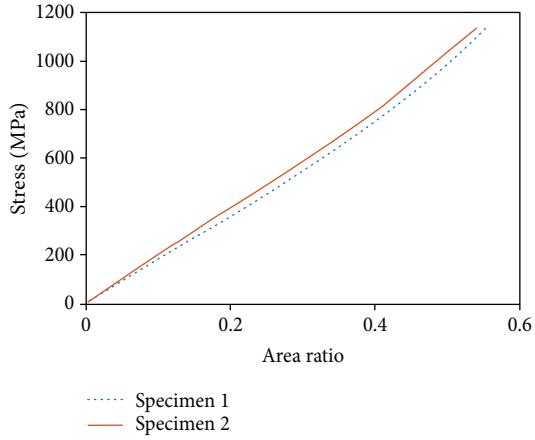

(b) Result of the sensor embedding test

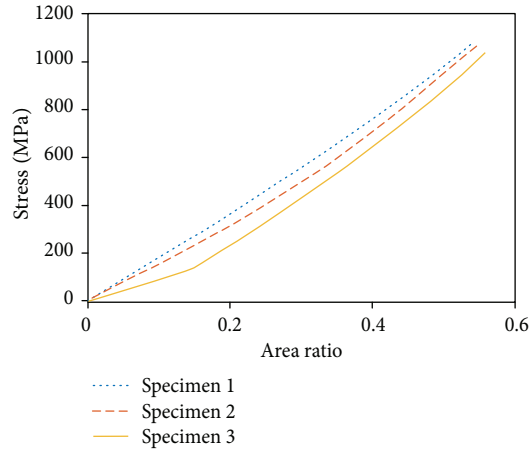

(c) Result for sensor no.1 of the scaled PSC girder test

Figure 17: Compensated results.

magnetic hysteresis was converted to the area ratio to compensate for the initial value of the embedded EM sensor caused by the differences in the number of turns and distribution of coils. The area ratio and tensile stress have almost similar relationship in spite of the difference in type, cross-sectional area of PS tendons, and sensors. According to the results of experimental studies, the embedded EM sensor could be applied to the PSC girder to measure the tensile force of PS tendons.

Data Availability

The magnetic hysteresis data used to support the findings of this study are included within the article.

Conflicts of Interest

The authors declare that they have no conflicts of interest.

Acknowledgments

This paper was supported by Samsung Research Fund, Sungkyunkwan University, 2018.

References

[1] K. L. Rens, T. J. Wipf, and F. W. Klaiber, "Review of nondestructive evaluation techniques of civil infrastructure," *Journal of Performance of Constructed Facilities*, vol. 11, no. 4, pp. 152–160, 1997.

[2] J. W. Kim, J. Kim, S. Park, and T. K. Oh, "Integrating embedded piezoelectric sensors with continuous wavelet transforms for real-time concrete curing strength monitoring," *Structure and Infrastructure Engineering*, vol. 11, no. 7, pp. 897–903, 2015.

[3] C. Lee, J. Kim, S. Park, and D. H. Kim, "Advanced fatigue crack detection using nonlinear self-sensing impedance technique for automated NDE of metallic structures," *Research in Nondestructive Evaluation*, vol. 26, no. 2, pp. 107–121, 2015.

[4] S. Park, J. W. Kim, C. Lee, and J. J. Lee, "Magnetic flux leakage sensing-based steel cable NDE technique," *Shock and Vibration*, vol. 2014, Article ID 929341, 8 pages, 2014.

[5] C. V. Shenoy and G. C. Frantz, "Structural tests of 27-year-old prestressed concrete bridge beams," *PCI Journal*, vol. 36, no. 6, pp. 80–90, 1991.

[6] B. O. Aalami, "Time-dependent analysis of post-tensioned concrete structures," *Progress in Structural Engineering and Materials*, vol. 1, no. 4, pp. 384–391, 1998.

[7] O. Onyemelukwe and S. Kunnath, *Field Measurement and Evaluation of Time-Dependent Losses in Prestressed Concrete Bridges*, Research Report (Project Number: WPI-0510735, Department of Transportation), Florida, FL, USA, 1997.

[8] H. L. Chen and K. Wissawapaisal, "Measurement of tensile forces in a seven-wire prestressing strand using stress waves," *Journal of Engineering Mechanics*, vol. 127, no. 6, pp. 599–606, 2001.

[9] G. A. Washer, R. E. Green, and R. B. Pond Jr, "Velocity constants for ultrasonic stress measurement in prestressing tendons," *Research in Nondestructive Evaluation*, vol. 14, no. 2, pp. 81–94, 2002.

[10] J. T. Kim, C. B. Yun, Y. S. Ryu, and H. M. Cho, "Identification of prestress-loss in PSC beams using modal information," *Structural Engineering and Mechanics*, vol. 17, no. 3_4, pp. 467–482, 2004.

[11] J. T. Kim, J. H. Park, D. S. Hong, H. M. Cho, W. B. Na, and J. H. Yi, "Vibration and impedance monitoring for prestress-

loss prediction in PSC girder bridges," *Smart Structures and Systems*, vol. 5, no. 1, pp. 81–94, 2009.

[12] J. M. Kim, H. W. Kim, Y. H. Park, I. H. Yang, and Y. S. Kim, "FBG sensors encapsulated into 7-wire steel strand for tension monitoring of a prestressing tendon," *Advances in Structural Engineering*, vol. 15, no. 6, pp. 907–917, 2012.

[13] C. Lan, Z. Zhou, and J. Ou, "Monitoring of structural prestress loss in RC beams by inner distributed brillouin and fiber Bragg grating sensors on a single optical fiber," *Structural Control & Health Monitoring*, vol. 21, no. 3, pp. 317–330, 2014.

[14] D. Makhnovskiy, A. Zhukov, V. Zhukova, and J. Gonzalez, "Tunable and self-sensing microwave composite materials incorporating ferromagnetic microwires," *Advances in Science and Technology*, vol. 54, pp. 201–210, 2008.

[15] M. Churyukanova, S. Kaloshkin, E. Shuvaeva et al., "Non-contact method for stress monitoring based on stress dependence of magnetic properties of Fe-based microwires," *Journal of Alloys and Compounds*, vol. 748, no. 5, pp. 199–205, 2018.

[16] M. L. Wang, G. Wang, and A. Zhao, "Application of EM stress sensors in large steel cables," in *Sensing Issues in Civil Structural Health Monitoring*, pp. 145–154, Springer, 2005.

[17] S. Sumitro, S. Kurokawa, K. Shimano, and M. L. Wang, "Monitoring based maintenance utilizing actual stress sensory technology," *Smart Materials and Structures*, vol. 14, no. 3, pp. S68–S78, 2005.

[18] J. Kim, J. W. Kim, C. Lee, and S. Park, "Development of embedded EM sensors for estimating tensile forces of PSC girder bridges," *Sensors*, vol. 17, no. 9, 2017.

[19] A. Zhukov, M. Vazquez, and J. M. Garcia-Beneytez, "Magnetoelastic sensor for signature identification based on mechanomagnetic effect in amorphous wires," *Journal de Physique IV*, vol. 8, pp. Pr2-763–Pr2-766, 1998.

[20] A. Zhukov, V. Zhukova, V. Larin, and J. Gonzalez, "Tailoring of magnetic anisotropy of Fe-rich microwires by stress induced anisotropy," *Physica B: Condensed Matter*, vol. 384, no. 1-2, pp. 1–4, 2006.